5 Magnetization Dynamics in Gd(0001)/W(110)

The growing interest in using magnetic materials for practical applications motivates our research on electron and spin dynamics of the 4f core shell of gadolinium. Most important technological applications are data storage and electronic switching. The development of magnetic switch elements, e.g. spin-filter and spin-transitors [Wol01, All02] stimulates extensive studies of spin dynamics in different magnetic materials.
Gadolinium is one of the prototype systems to study magnetization dynamics with the ultimate goal to understand the microscopic interaction and coupling between the quasiparticles, e.g. electrons, phonons and magnons upon laser excitation.

Two powerful methods to study the magnetic and electronic structure of solids are spin-resolved two-photon photoemission and spin-resolved photoelectron spectroscopy. Here, the spin of the outgoing photoelectron is monitored in addition to the parameters ($k_{\parallel}$,E) measured in conventional photoemission. A disadvantage of these methods is the low efficiency [Pie88].
Magnetic dichroism (MD) in photoemission is an alternative way to obtain information on the magnetic state of the sample. MD in core-level photoemission was for the first time observed by Baumgarten *et al.* [Bau75], who performed angle-resolved measurements using circularly polarized light. MD is also observable with linear light [Kru04]. In this chapter only the magnetic linear dichroism (MLD) will be explained.
The following Section 5.1 outlines the electronic structure of gadolinium. Section 5.2 presents the experimental details of this study including the preparation of gadolinium films. Successively, Section 5.3 shows the static measurements to characterize and improve the MLD in gadolinium. Finally the main part of this study is reported in Section 5.4 which describes the time-resolved experiment.
The main motivation of this chapter is to understand how the magnetic order in the Gd 4f level is affected upon excitation of the valence band electrons with a femtosecond (fs) laser pulse and what is the Gd 4f contribution to the total magnetization of the sample.

5.1 Electronic Structure of Gadolinium

The metal gadolinium belongs to the lanthanide group and crystallizes in the hcp-structure with the lattice constant $a = 3.629$ Å and $c/a = 1.597$ [Leg80]. The unique electronic and magnetic properties of gadolinium result from the partially filled 4f shell. Gadolinium is a ferromagnet with localized magnetic moments (Heisenberg ferromagnet), where the half filled 4f shell (S=7/2, L=0) gives rise to the large localized magnetic moments of $\simeq 7\ \mu_B$[1] per lattice site (Fig. 5.1).
The polarization of the conduction electrons by the 4f moments leads to an indirect exchange mechanism, in which the delocalized valence-band electrons mediate interaction between the localized 4f moments via the so-called Rudeman-Kittel-Kasuya-Yosida (RKKY) indirect exchange interaction (Appendix B).

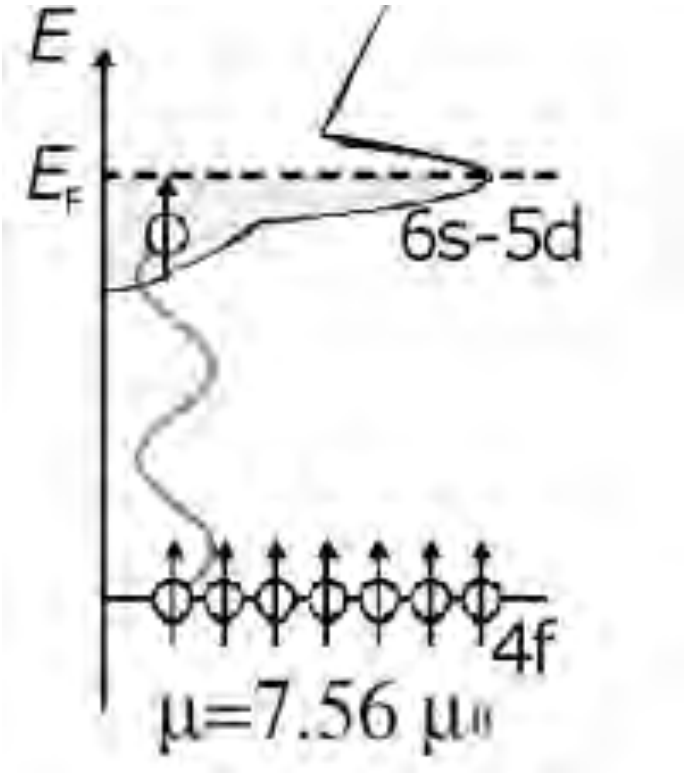

Figure 5.1: Schematic picture of the electronic system of gadolinium. The density of energy levels of the delocalized 5d6s valence band is shown and the Gd 4f shell. The Gd 4f polarized the electrons in valence band.

The electronic structure of gadolinium in the ferromagnetic phase includes two bands of majority and minority electrons at T = 0 K. Figure 5.2 represents the

[1] μ_B=9.27 · 10^{-24} Am^2

surface-projected band structure for the Gd(0001)-surface, calculated by density functional theory [Kur02]. The conduction band Δ_2 is formed by the 5d6s-electrons (3-electrons per atom). The occupied 4f core-level lies 8 eV below the Fermi level E_F outside of the range plotted in the graphic 5.2 [Wes95]. The unoccupied multiplet of the 4f level lies approximately 4 eV above E_F [Wes95].

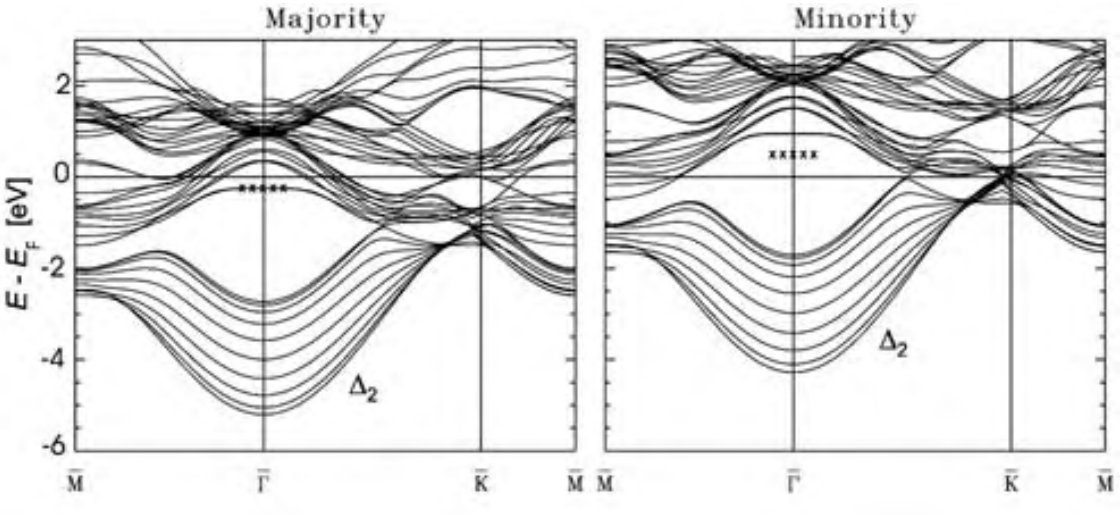

Figure 5.2: Band structure of Gd(0001)-surface at T=0 K, calculated by density functional theory (FLAPW, LDA + core approximation) from [Kur02]. Left: The majority levels, right the minority levels. Dots indicate the experimentally determined position of the Gd(0001) surface state.

5.1.1 Thermalization, Heat Transport and Two-Temperature Model

In thermal equilibrium the electrons follow the Fermi-Dirac distribution with the distribution function:

$$f(E;\mu,T) = (e^{(E-\mu)/k_B T} + 1)^{-1} \tag{5.1}$$

By the absorption of a light pulse with photon energy $h\nu$ the electrons from occupied states below the Fermi level E_F are excited to the unoccupied states above E_F. Figure 5.3a displays the electron distribution at the initial time $t_0 = 0$ after the arrival of the light pulse. Electrons close to E_F are excited in a one photon process by $h\nu$ above E_F. The width of the rectangle is $h\nu$, while its height depends on the excitation intensity. This strongly non-thermal electron distribution is converted back to a Fermi-Dirac distribution by scattering processes among the electrons themselves (electron-electron scattering) and with the lattice (electron-phonon scattering). Once thermal equilibrium among hot electrons is reached, a second time interval starts where electrons are characterized by the Fermi distribution (Fig. 5.3b)

and a temperature which in the beginning differs strongly from the lattice temperature. Driven by heat transport, hot electrons diffuse into deeper parts of the bulk. The diffusion length is governed by electron-phonon coupling which cools the electron bath. Diffusive electron motion and cooling by electron-phonon coupling can be well described by the two-temperature model. One can define a third time interval in which electrons and lattice have reached thermal equilibrium (Fig. 5.3c). According to [Fan92, Ret02], the thermalization time is shorter for more intense optical excitation. By electron-phonon scattering only a small energy transfer of typically 10 meV takes place. Therefore, mainly e-e scattering is responsible for the thermalization of the electronic system. Nevertheless, even during the thermalization a significant energy transfer and diffusional transport can occur. So the electronic system cannot be treated separately during the thermalization process.

Heat Transport

The present section explains the heat transport and the lattice temperature after laser excitation. The energy flow after an optical excitation is denoted heat transport, which is modeled by a diffusive contribution (the thermalized quasiparticle) and by a ballistic transport contribution (non-thermal quasiparticle). The heat transport in the metal and the transfer of heat to the phonon bath is described by,

$$\frac{dU_{el}}{dt} = \frac{\partial}{\partial z}(K_e \frac{\partial}{\partial z} T_{el}) - H(T_{el}, T_{ph}) + P(z,t) \tag{5.2}$$

$$\frac{dU_{ph}}{dt} = H(T_e, T_{ph}) \tag{5.3}$$

The energy of the electron gas with temperature T_{el} is [Ash76]:

$$U_{el} = \frac{1}{2}\ \gamma_{el}\ T_{el}^2 \tag{5.4}$$

where γ_{el} is the electronic heat-capacity coefficient. Equation 5.2 describes the change in the energy of the electronic system with the time dU_{el}/dt. By absorption of the laser pulse $P(z,t)$ the energy transfer from the electronic system to the lattice is $H(T_{el}, T_{ph})$. The electron thermalization proceeds by electron-electron scattering, electron-phonon coupling and diffusive motion. This model is simplified assuming that the illuminated surface area is much bigger (several micrometer) than the optical penetration depth in metals (several nanometer). Therefore, the lateral heat gradient is neglected and a one-dimensional problem is considered:

$$T_{el} = T_{el}(z,t), \qquad T_{ph} = T_{ph}(z,t), \qquad U_{el} = U_{el}(z,t), \qquad U_{ph} = T_{ph}(z,t). \tag{5.5}$$

Equation 5.3 describes the energy of the phonon system, which can be represented as a function of the phonon temperature and the phonon heat capacity:

$$U_{ph} = \int_0^{T_{ph}} dT\ C_{lat}(T) \tag{5.6}$$

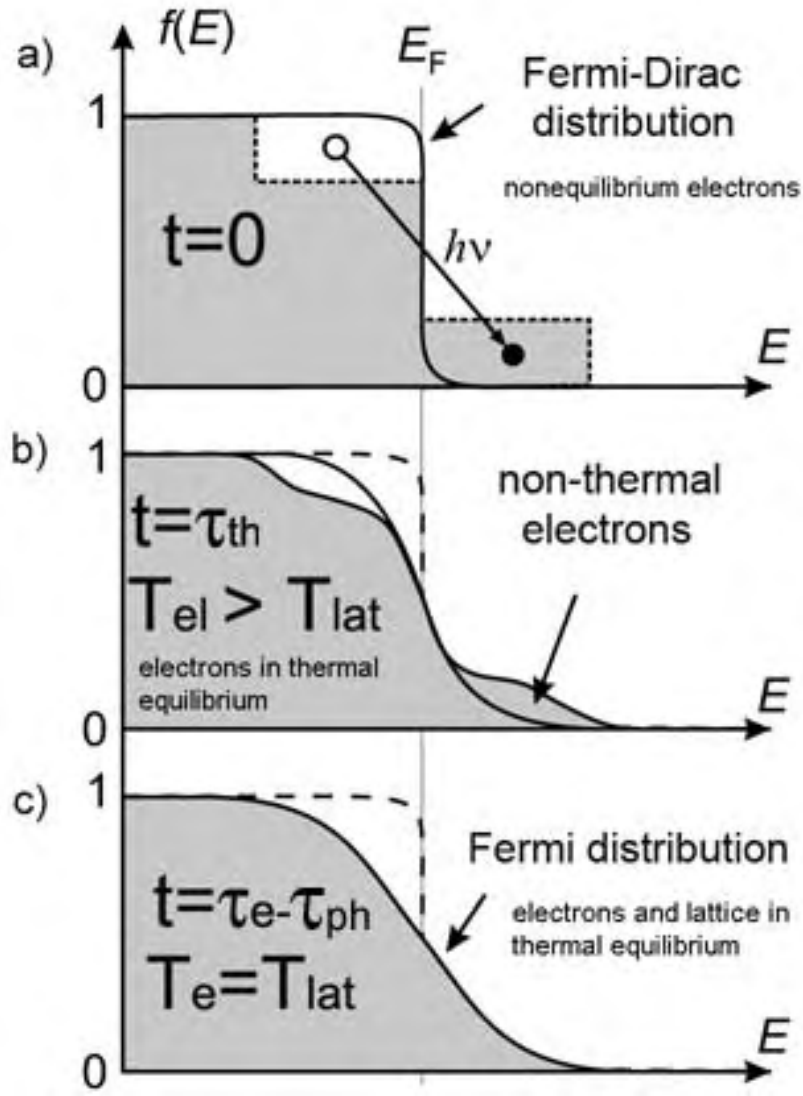

Figure 5.3: Thermalization of an electron gas by optical excitation. a) Optical excitation of electrons is pictured by the dislocation of a rectangle above the Fermi level, E_F at t=0. b) At t=τ_{th} electrons have equilibrated by electron-electron scattering forming a Fermi distribution with a well defined electron temperature T_e, and diffusive energy transport starts within the electron gas. c) Via electron-phonon coupling the electrons equilibrate with the lattice at t=$\tau_{el-\tau ph}$, energy transport now proceeds via thermal diffusion.

The phonon heat capacity is described by the Debye model [Lis04].

Figure 5.4 displays the specific heat of a gadolinium film versus temperature from experimental data [Sch81, Dan98] (open circles) and the Debye model θ_D with a Debye temperature of T_D=163 K.

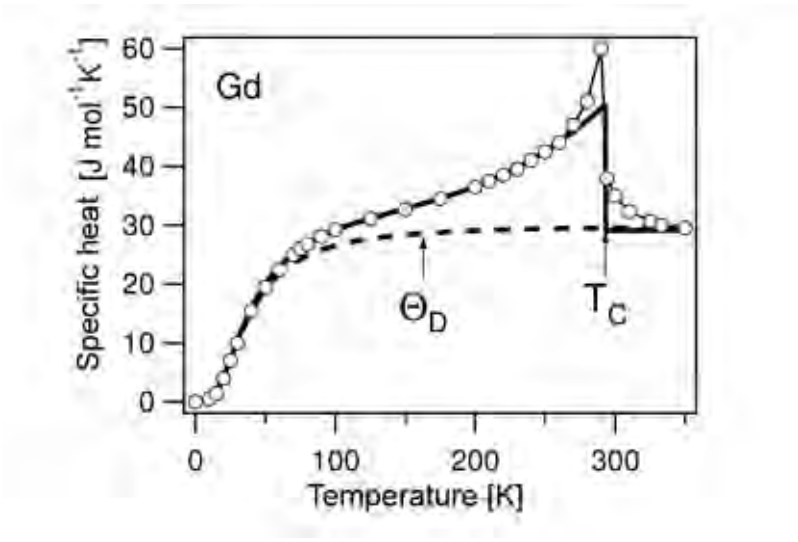

Figure 5.4: Heat capacity of gadolinium from Debye model (eq. 5.6) with a Debye temperature of 163 K and a Curie temperature 293 K. Experimental data (∘) from [Sch81, Dan98].

The specific heat for a ferromagnetic material is bigger than for a paramagnetic material, because additional energy is required to reduce the magnetic ordering. The solid line in Fig. 5.4 is an empiric model function from Ref. [Lis05], consisting of the sum of the lattice specific heat C_{lat} from the Debye model and the magnetic contribution C_m:

$$C_V = C_{lat} + C_m \tag{5.7}$$

Two-Temperature Model

Due to the vastly different heat capacities of electrons and lattice the equilibrium temperature of the lattice rise is generally one to two orders of magnitude smaller than for electrons. Thermal equilibrium among the excited electrons is reached within several hundred fs, depending on the excitation energy above Fermi level. Once it is established, we encounter the physical situation of a hot electron bath in a cold lattice which can be described by two separated temperatures, T_e and T_{lat}. Cooling of the electrons proceeds by electron-electron scattering, electrons scatter among each other, electron-phonon coupling and by diffusive motion. The temperature relaxation in time and sample depth can be modeled by two coupled diffusion equations, one describing the heat conduction of electrons and the other for the lattice. Both equations are connected by a term that is proportional to the electron-phonon coupling constant g and to the temperature difference between electrons and lattice. The assumption that the electron-phonon coupling can be lumped into one linear coupling term of the form $g \cdot (T_e - T_{lat})$ is the essence of the

two-temperature model (TTM), originally proposed by Anisimov et.al. [Ani74]. It can be written in the following form:

$$C_e(T_e)\frac{\partial T_e}{\partial t} = \frac{\partial}{\partial z}(K_e\frac{\partial}{\partial z}T_e) - g(T_e - T_{lat}) + P(\mathbf{r},t) \tag{5.8}$$

$$C_{lat}\frac{\partial T_{lat}}{\partial t} = g(T_e - T_{lat}) \tag{5.9}$$

$$\tag{5.10}$$

Here, C_e and C_{lat} are the respective heat capacities of electrons and lattice and K_e is the thermal conductivity of the electrons. The heat conduction of the lattice was neglected. The optical excitation term:

$$P(\mathbf{r},t) = \frac{\alpha A I(\mathbf{r},t)e^{-\alpha z}}{1 - e^{-\alpha d}} \tag{5.11}$$

describes the absorbed energy density, determined by penetration depth is l α^{-1}, film thickness d, and the absorbed fraction of the incident intensity $A \cdot I(\mathbf{r},t)$, with A=(1-R-T). Here, R and T denoted reflectivity and transmissivity, respectively.
The TTM can be solved numerically to predict the time dependence of T_e and T_{lat}.

5.1.2 Ferromagnetism

A ferromagnet has a spontaneous magnetic moment **M** below the Curie temperature T_c even in the absence of an external magnetic field. The existence of a spontaneous moment suggests that spins are arranged in a regular manner:

$$\mathbf{M} = \frac{1}{V}\sum_i \mu_{\mathbf{i}} \tag{5.12}$$

The magnetic interaction is described by exchange interaction between localized electrons at the atom. The exchange interaction in the Heisenberg model is expressed by the spin operators of the electrons responsible for the magnetization.
The geometric configuration of the solid influences the total magnetic moment and its ordering. It is experimentally observed that a ferromagnet can be magnetized more easily along a certain crystallographic direction [Far98]. One finds so-called easy, intermediate and hard axes of magnetization. The energy difference associated with different directions of **M** defines the magnetic anisotropy energy, consisting of dipole-dipole interactions and the spin-orbit coupling. For Gd(0001) films on W(110) ferromagnetic resonance (FMR) shows that the easy axis lies in-plane.
The ferromagnetic/paramagnetic phase transition in Gadolinium occurs at the Curie temperature T=293 K. Understanding the relation between electronic and magnetic properties at finite temperature leads to two limiting cases, the Stoner [Sto36] and spin-mixing [Kor77] model. The Stoner model predicts that the exchange splitting

of delocalized states, describing itinerant electrons, parallels the temperature dependence of the magnetization. The spin-mixing model pictures the magnetization of strongly localized systems where thermal fluctuations (spin-waves) reduce the magnetization. Nevertheless, lanthanides can be better modelled via spin mixing. Neither model exactly describe the temperature dependence of the magnetization.

The Stoner Model and Spin Mixing

Within the *mean-field-approximation* the exchange interaction between the electrons of the valence band (6s5d) and the localized 4f electrons, are aligned in an effective magnetic field $\mathbf{B}_{eff}$. The band structure splits in two bands (subsystems) with spin parallel and antiparallel to the magnetization (Fig. 5.5). The difference in energy of these bands is the exchange splitting Δ_{ex}. The Stoner model is used to describe

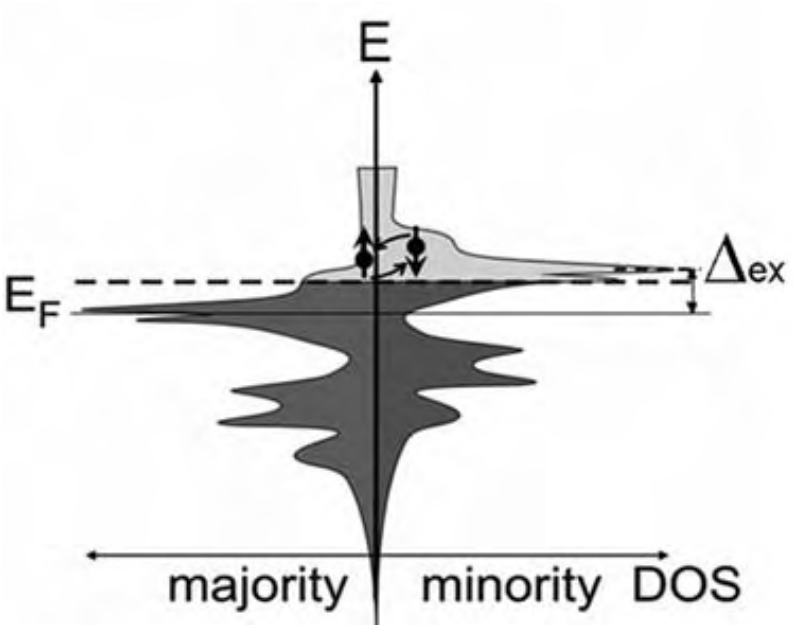

Figure 5.5: Sketch of the density of electronic states (DOS) in a ferromagnet described by the Stoner model. The levels split into majority and minority parts shifted by the exchange splitting Δ_{ex}.

systems with delocalised electrons, so-called itinerant ferromagnet . Above the Curie temperature the spin orientation disappears by thermal excitation. In general, the temperature dependence of the magnetization below the Curie temperature can be written as

$$M = M_S(1 - T/T_c)^{\beta} \tag{5.13}$$

where M_S is the magnetization at T=0 K, T_c the Curie temperature and β is the critical exponent. The value of the exponent depends on the dimension and the

exchange interaction. For lower temperatures, the magnetization follows the Bloch-law [Iba93]:

$$M = M_S(1 - a \cdot T^{3/2}) \tag{5.14}$$

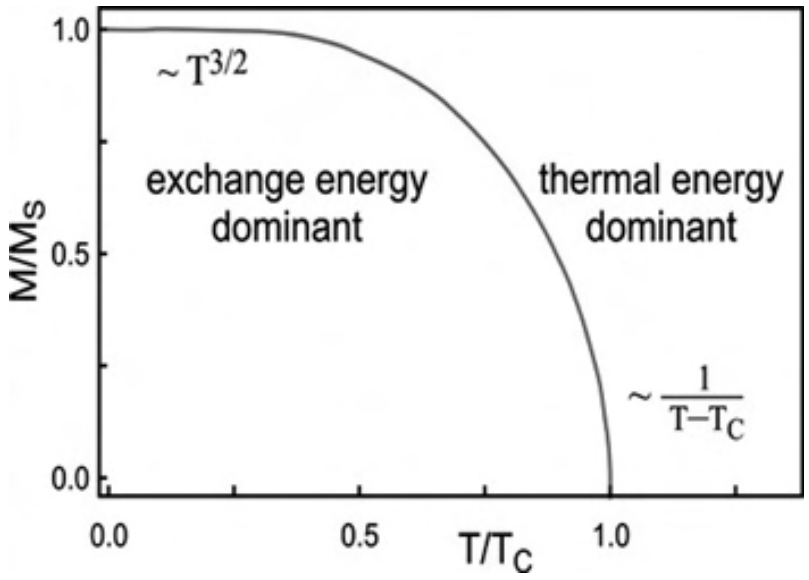

Figure 5.6: Magnetization of a ferromagnet below the Curie temperature

Figure 5.1 shows a schematic electronic energy diagram for gadolinium. Strongly localized electrons of the 4f shell polarize by exchange interaction delocalized electrons in the conduction band (6s5d). The ferromagnetism in gadolinium can be described by an effective Heisenberg model (Appendix B). The interaction between 4f electrons and conduction band can be explained by the so-called s-f model [Nol79], where the 4f electrons polarize the itinerant electrons of the valence band. Ab initio calculations show that a transition from a single-particle to a many-particle picture does not allow to shift the energy of electrons [Rex99]. An electron from the conduction band interacts by emission or absorption of magnons with the electrons of the 4f shell. Particularly, a majority-electron flips its spin and becomes a minority electron by emission of a magnon.
The quasi particle density of states (QDOS) is sketched in Fig. 5.7 for different temperatures. At low temperatures (left), the majority and the minority bands are then split at a certain energy, similar as in the Stoner model. At high temperatures (center) the spectral density changes. The quasiparticle flips its spin by quasielastic emission or absorption of a magnon. At the Curie temperature (right), the density of energy levels are the same for both spins. The magnetic order is lost, and the spin polarization disappears:

$$P = \frac{N\uparrow - N\downarrow}{N\uparrow + N\downarrow} \tag{5.15}$$

where N↑ and N↓ is the number of electrons with spin up and down at a certain energy.

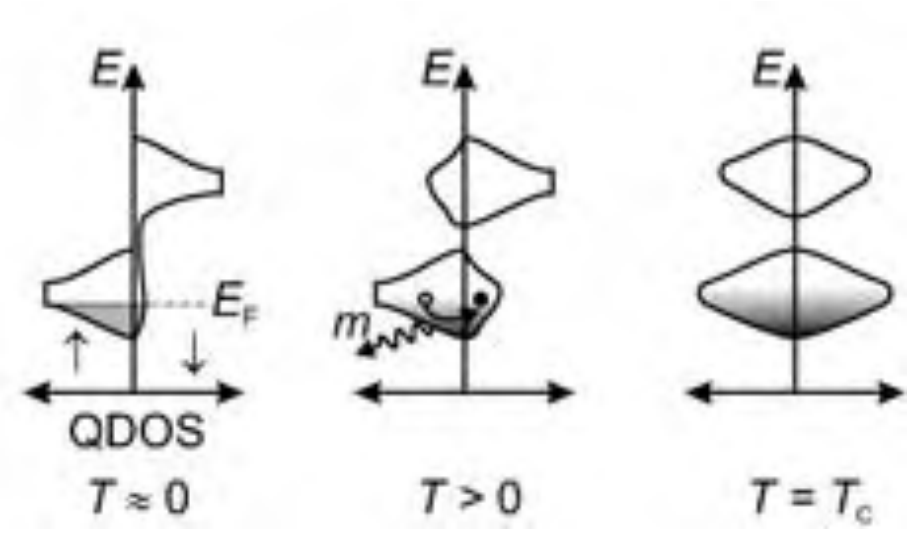

Figure 5.7: Sketch of the quasi particle density of states (QDOS) in the spin-mixing model for electrons in the conduction band, which have delocalized magnetic moments and couple by exchange interaction. Left: At low temperature the majority and the minority electron bands are shifted similar as in the Stoner model. Center: At high temperatures, a majority electron can flip its spin and emit a magnon. Right: At the Curie temperature, both bands have the same occupancy, so the spin polarization vanishes [Rex99].

5.1.3 Characterization of the Gadolinium (0001) Surface State

The gadolinium film preparation will be explained in the next section. Different measurements have been done to characterize the film and to control film preparation. Surface-state and valence-band photoemission-spectroscopy provide information about the quality of the gadolinium surface and bulk. Angle-resolved photoemission spectra of the gadolinium valence-band with $\pm$ 1° angular acceptance and an energy resolution of 30 meV are realized. The most intense peak close to the Fermi level is found for normal emission ($\vartheta = 0°$) and represents the Gd(0001) surface state (c.f. Fig. 5.2). With increasing emission angle the surface state disperses higher binding energy due to hybridization the delocalized 5d6s valence-band.

The effect of a magnetization reversal on the surface-state binding energy is plotted in Fig. 5.8. For off-normal emission $\vartheta = 0°$ the position of the surface state changes, while in normal emission the peak position is the same for both magnetization directions.

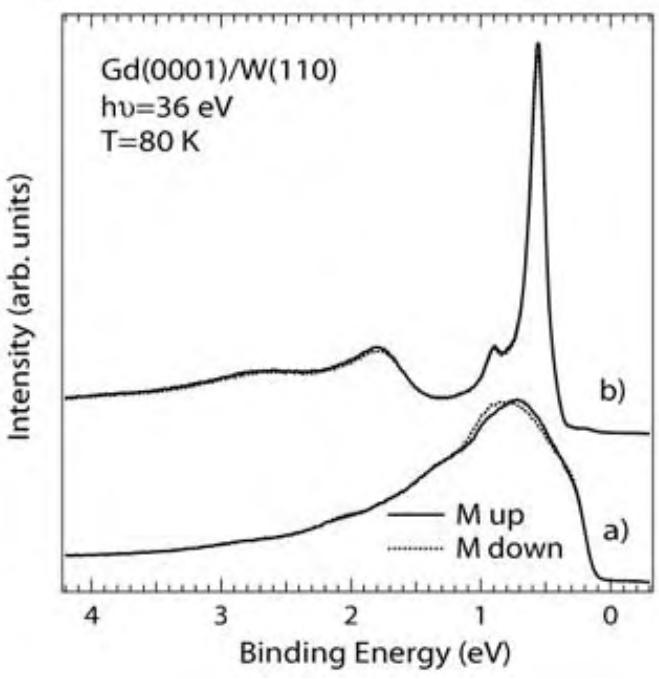

Figure 5.8: Effect of magnetization reversal (dot and solid curves) on the peak position of the Gd(0001) surface state in the (a) off-normal emission and (b) normal emission photoemission spectrum.

5.2 Experimental Setup

This section describes sample preparation, experimental procedures, and photoemission geometries.

5.2.1 Sample Preparation, Sample Holder and Magnetic Coils

Studies of the electronic and magnetic structure of crystal surfaces require samples of high structural and chemical quality. Gadolinium as well as other rare-earth metals are especially demanding due to their high chemical reactivity. The electronic and magnetic properties of a freshly prepared surface will be altered substantially within only several hours, even in ultra-high vacuum with residual pressures below 10^{-10} mbar.

Tungsten Substrate

High-quality lanthanide samples are best prepared by epitaxial growth on an appropriate substrate, typically a tungsten single crystal.

The W(110) surface is particularly well suited as a substrate for the growth of monocrystalline gadolinium films for the following reasons:

- the high surface energy of the substrate ensures wetting and epitaxial growth;
- bbc W(110) lattice constant matches rather well with that of the (0001) surface of the hcp lattice, causing therefore only small lattice distortions;
- tungsten is stable against the formation of intermetallic compounds with gadolinium. This allows one to anneal the films without problem of alloy formation;
- the cleaning procedure of W(110) is fast and well known [Kru04, Lis05];

The dimensions of the tungsten-crystal used in the present setup were 9 mm diameter with a thickness of 3.2 mm. The principal contaminant of tungsten is carbon. It is removed from the tungsten crystal by heating the crystal in an oxygen atmosphere of 10^{-6} mbar at 1800 K. Under these conditions carbon diffuses to the surface where it forms CO and CO_2, which desorb from the surface at this temperature. Residual oxygen from this procedure can be removed by subsequent heating of the tungsten crystal for a few seconds to 2000 K. Likewise, the gadolinium film can be removed by such a short flash.
The quality of the gadolinium film depends on the preparation conditions, in particular on the evaporation rate, the substrate and annealing temperatures.

Gadolinium

Gadolinium single-crystal films are prepared by vacuum deposition from high-purity gadolinium metals using a home-built evaporator. Pieces of gadolinium metal (99.99% purity) from ChemPur in Karlsruhe, are put into a crucible heated by electron bombardment. The usual evaporation rate was 5 Å/min as monitored by a quartz microbalance. The temperature of the substrate during evaporation was held at 320 K. After deposition the sample was annealed up to 750 K for 10 minutes to improve the quality and ordering of the film. The annealing temperature depends on the film thickness and is about 750 K for 10 nm thick films. For higher annealing temperatures the film breaks up into islands [Asp94].

Sample Holder

Using a tungsten crystal as substrate for gadolinium films imposes several demands on the sample holder. The temperature range for the sample holder is between 30 to 2500 K and a careful temperature measurement has to be included. In addition to prevent any remanent magnetic field near the sample, magnetic materials must be avoided in the vicinity of the sample holder.
The sample holder used in this work is shown in Fig. 5.9. The sample is held by

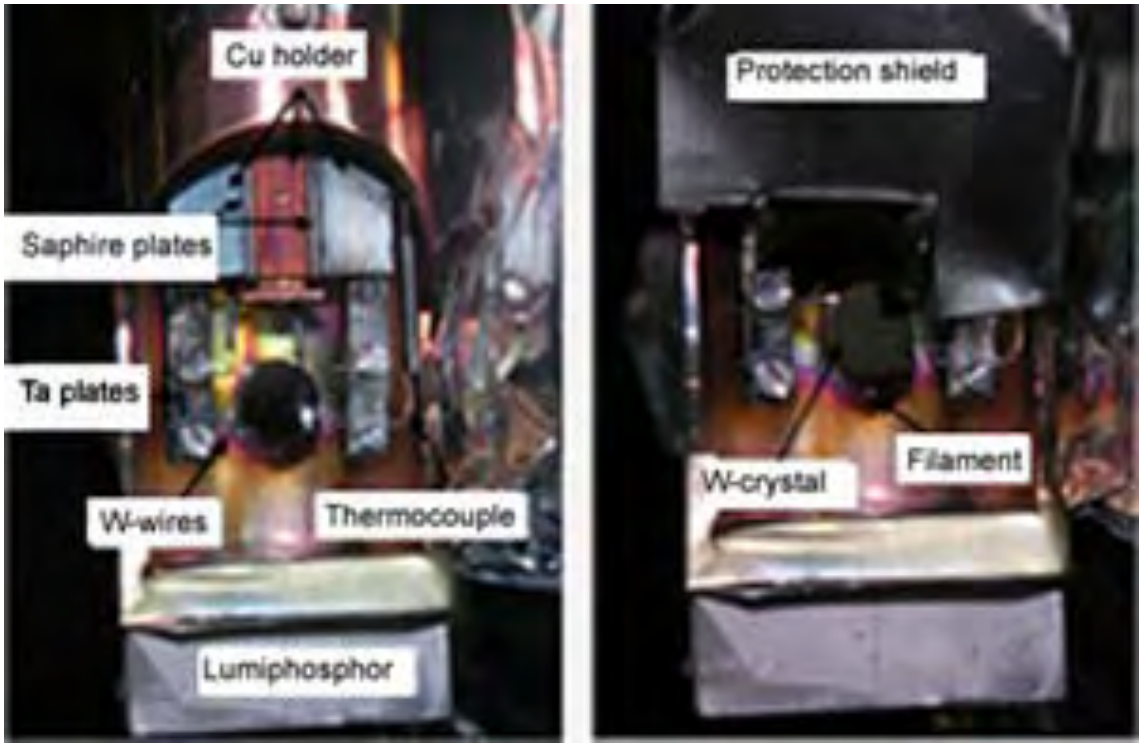

Figure 5.9: Schematics of the gadolinium holder with a commercial liquid Helium/Nitrogen cryostat.

two tungsten wires (∅ 0.38 mm) fixed between two copper rods, which are conceted through sapphire plates to the cold block of a liquid-Helium or nitrogen flow cryostat. Fixed in this way, the crystal is electrically isolated from the cryostat. Single-crystalline sapphire has a good thermal conductivity at low temperatures, and it is a poor thermal conductor at higher temperatures. The construction in Fig. 5.9 allows to reach low temperatures down to 30 K and to flash the sample to 2000 K. Crystal heating is achieved by electron bombardment from the back of the crystal (for high temperatures) or by resistive heating (for lower temperatures).
A W/Re type C (W5%Re/W26%Re) thermocouple is inserted in a hole at a side of the crystal and fixed by a tungsten-wire to the crystal to provide good thermal contact. The lumiphosphor in Fig. 5.9 is used to improve the spatial overlap between laser and synchrotron beam spots finding on the same plane than the sample.

Magnetic Coil

To magnetize the sample, it is placed into a Helmoltz arrangement of two electric coils (c.f. Fig. 5.10). A current of 10 A produces a field of 170 Oe at the sample position and changing the direction of the current allows to switch the magnetic-field direction. To reduce the influence of small residual fields the chamber and the

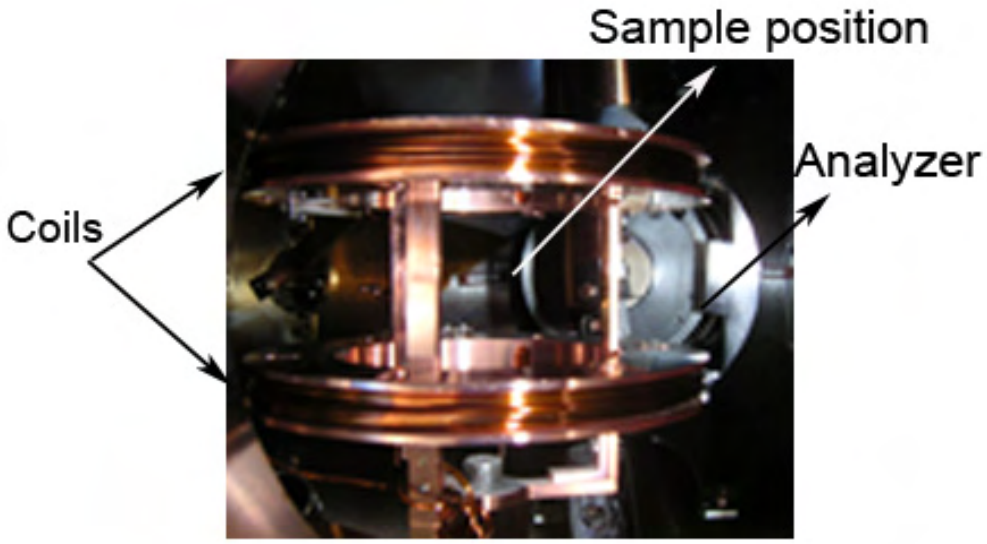

Figure 5.10: Set of copper magnet coil used to provide a homogeneous magnetic field.

analyzer lens is covered with a μ-metal shield.

5.2.2 Experimental Geometry

The study of the spin dynamics of the 4f core-electrons in Gd(0001) was performed at U125/1 PGM at BESSY. The synchrotron and laser light was linearly p-polarized impinging nearly collinear on the sample. The sample was magnetized perpendicular to the scattering plane (Fig. 5.11). The linear dichroic signal depends on the angle between the incoming light ($\vec{E}$), the magnetization direction ($\vec{M}$) and the emission angle of the photoemitted electrons ($\vec{K}$) according to the Eq. 5.16. The incoming light was set by the fixed geometry of the synchrotron beamline and the endstation. The magnetization direction lies in plane, so that the only parameter left to improve the dichroic contrast was the emission angle of the photo-electrons. The experimental UHV system used for this study is described in Chapter 2, Section 2.2.4. An extra manipulator was implemented to hold and prepare the gadolinium film. To determine the zero of the time delay between laser and synchrotron pulses the surface photovoltage at clean silicon was measured following the procedure steps, mentioned in Section 2.4.

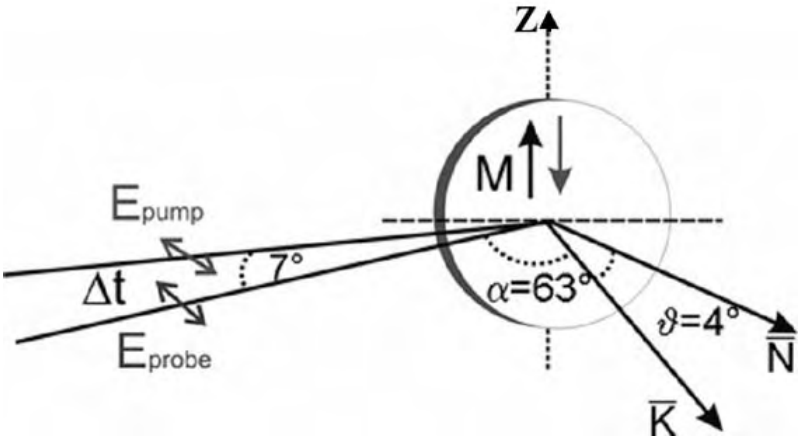

Figure 5.11: Experimental geometry laser-pump and synchrotron-probe pulses are both p-polarized and enclose an angle of 7°. The angle of incidence is $\alpha = 63^{\circ}$ with respect to the surface normal. Photoelectrons are detected at an emission angle of $\vartheta = 4^{\circ}$ with respect to the surface normal.

5.3 Magnetic Dichroism in Photoemission

A way to obtain information about the magnetic state of the sample is magnetic linear dichroism (MLD), observed for the first time by Roth *et al.* [Rot85] in Fe 3p core-level photoemission. Magnetic dichroism in photoemission originates from the fact that dipole-transition matrix elements depend on the magnetic quantum number of the electron in the initial state and parameters of the incident radiation, such as polarization and angle of incidence. Different choices of the incident radiation field and initial state will lead to different transition probabilities into a particular final state. Therefore, in appropriately chosen experimental geometries a change in sample magnetization $\overrightarrow{M}$ and linear polarized electron field $\overrightarrow{E}$ will lead to a variation of photoemission line shape and position, commonly referred to as magnetic linear dichroism in photoemission.
The linear magnetic dichroism can thus be used as a signature for the magnetic order of the 4f spin system.

5.3.1 Introduction to Magnetic Dichroism

In magnetic dichroism photoemission experiments one needs three quantities to define the system:

$$\{\ \overrightarrow{E}, \overrightarrow{M}, \overrightarrow{K}_{em}\}$$

Vector $\overrightarrow{E}$ describes the incoming radiation, the polarization of the light. $\overrightarrow{M}$ is the magnetization of the sample and $\overrightarrow{K}_{em}$ the emission direction of the photoelectrons.

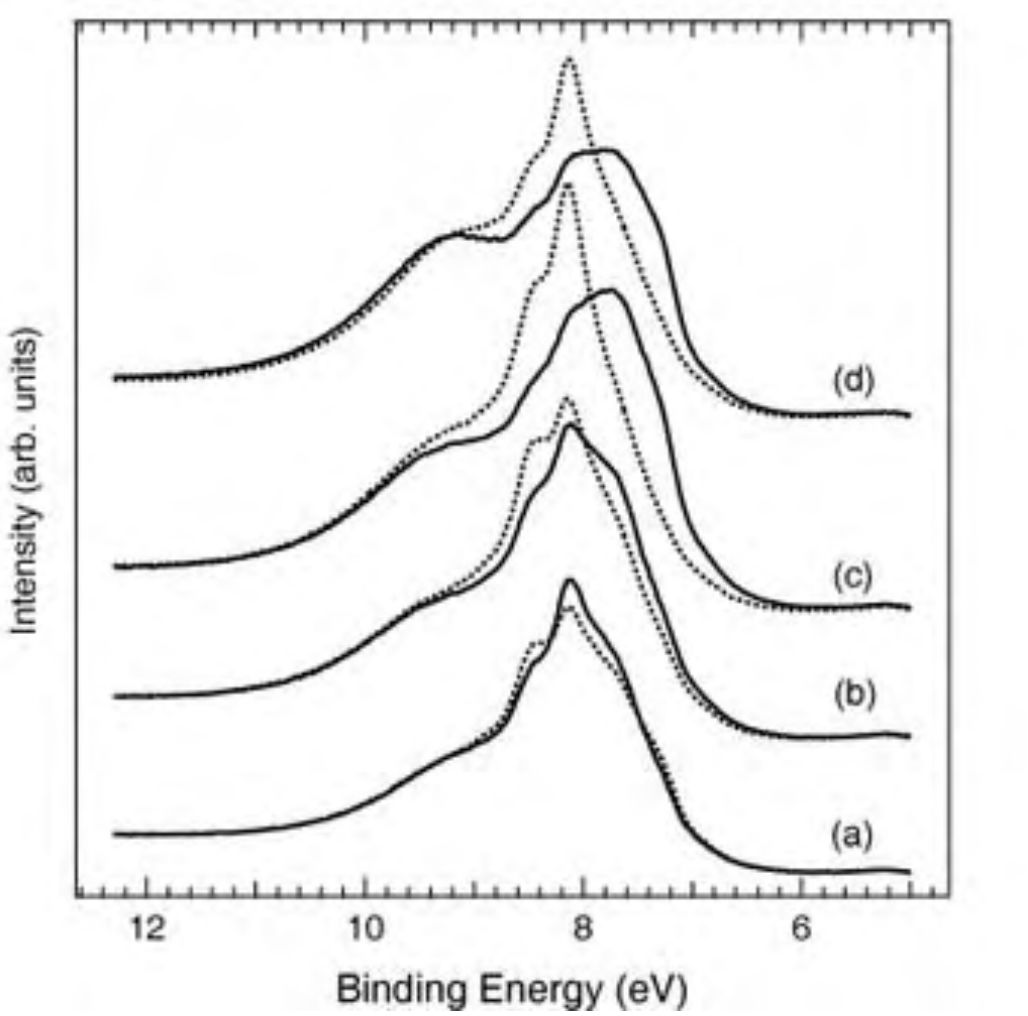

Figure 5.12: Photoemission spectra of the Gd 4f core-level for a 100 Å thick of Gd(0001) film on W(110), recorded for different emission angles: a) 6°, b) 0°, c) -2°, d) -8°. In the experimental geometry shown in Fig. 5.11 pairs combine spectra for opposite magnetization directions (doted lines correspond to magnetization up and solid lines to magnetization down).

According to Feder and Henk [Fed96], a necessary condition for the presence of MD effects in a particular geometry is that no space-symmetry operation exists which reverses the magnetization but leaves the system unchanged otherwise. For the geometry of our setup (Fig. 5.11), the MLD arises since there is no symmetry operation of the C_{3v} point group of the (0001) hcp-plane which allows to restore the experimental geometry upon a reversal of the axial vector of the in-plane magnetization. Magnetic dichroism in photoemission can be observed with linearly p-polarized light (described by $\overrightarrow{E}$), when the vectors span a chiral geometry [Tho94, Rot85, Sir94],

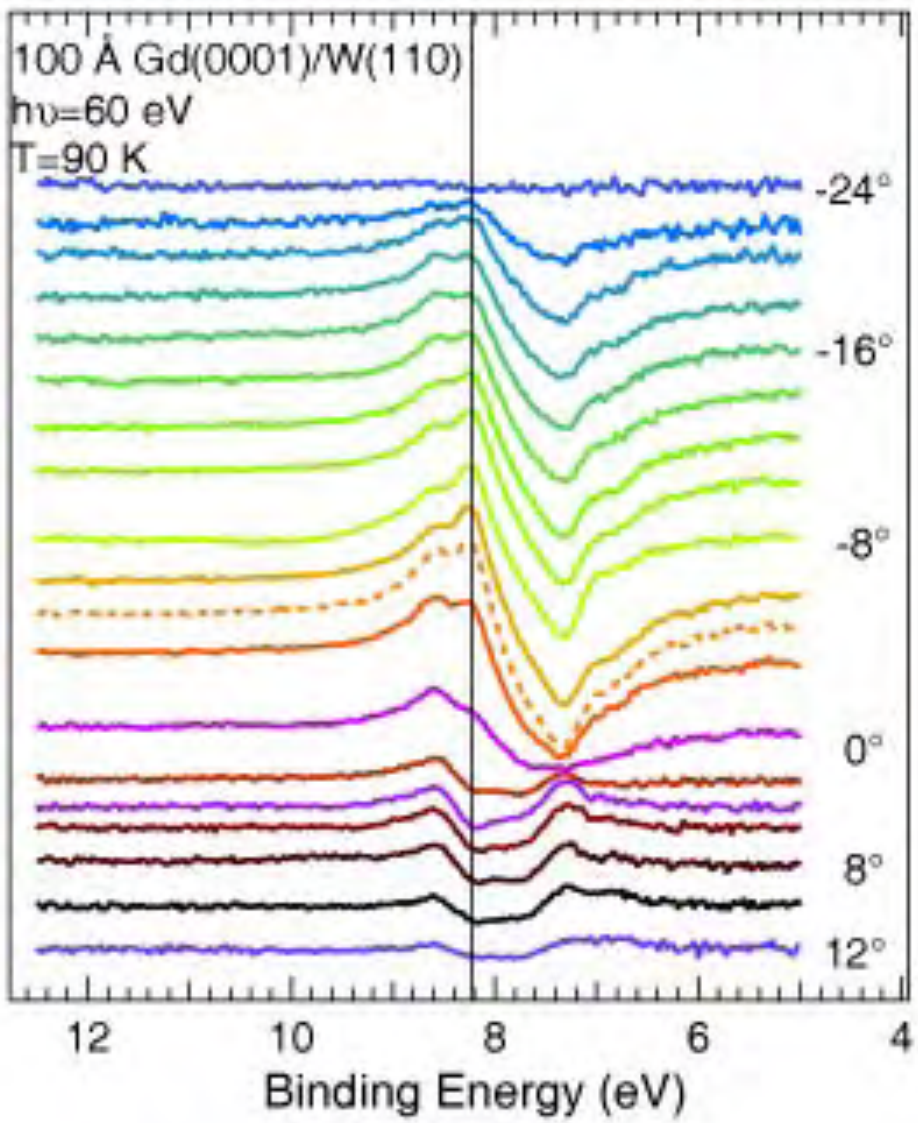

Figure 5.13: Angle-resolved photoemission MLD spectra of the Gd 4f core-level for a 100 Å thick film of Gd(0001) on W(110). MLD signal for emission angles around normal emission, recorded with a constant step width of 2° between individual spectra. Spectra were recorded at a temperature of 90 K.

i.e. when

$$|\vec{E}(\vec{M} \times \vec{k})| > 0 \tag{5.16}$$

Both synchrotron and laser pulse impinge on the sample nearly collinear, the magnetization of the sample was in the plane parallel to the surface the z-axis, (Fig. 5.11). A detailed analysis of magnetic dichroism was in a one-electron model given

by Menchero [Men98]. Although the many-body approach is commonly accepted to describe better the photoemission signal from the 4f shell.

5.3.2 Magnetic Dichroism of the Gd-4f shell

In the ground state seven electrons occupy the Gd-4f shell and the shell is half filled. According to Hund's rules and using the LS coupling scheme of Ref. [Kru04], the orbital angular momenta are coupled to the total angular orbital momentum L=0, and all spins are aligned to give the maximum value of the total spin S=7/2. The total angular momentum is J=7/2.

Gd(0001) on W(110)

The photoemission spectra of the 4f shell of Gd(0001), recorded with linearly p-polarized light with a photon energy of 60 eV in the experimental geometry of Fig. 5.11 show significant changes upon magnetization reversal due to the dichroic effect [Sta92]. Figure 5.12 shows photoemission spectra of the Gd 4f core-level. Evidently, the shape of the 4f spectrum is strongly modified upon variation of the emission angle. Four pairs of spectra are plotted for emission angles $\overrightarrow{K} = 6^{o},\ 0^{o},\ -2^{o},\ -8^{o}$.

A systematic variation of the MLD calculated according to $(I \uparrow - I \downarrow)/2$ is shown in Fig. 5.13. In spectra taken at positive values of the emission angle $\overrightarrow{K}$ the MLD vanishes rapidly compered with negative values of the emission angle. These significant variations in the MLD spectra demonstrate the large change in the magnetic components of the photoemission spectra from gadolinium, in both shape and intensity of the 4f peak. No distinction between bulk and surface component has been made. The systematic study of the MLD was done to find out the best experimental conditions for the time-resolved experiment, which will be explained in the following section.

Temperature Dependence

Figure 5.14 shows the photoemission spectra of the Gd 4f core-level for different temperatures and for both magnetization directions. For lower temperatures of approximately 100 K, both spectra present the maximum MLD when the magnetization is reversed. The MLD decreases when the temperature increases up to temperatures close to the Curie temperature where it disappears completely.
The temperature dependence of the magnetic dichroism has been evaluated to check whether it represents the magnetic state of the sample. The result is summarized in Fig. 5.15 and indicates a typical ferromagnetic behavior.

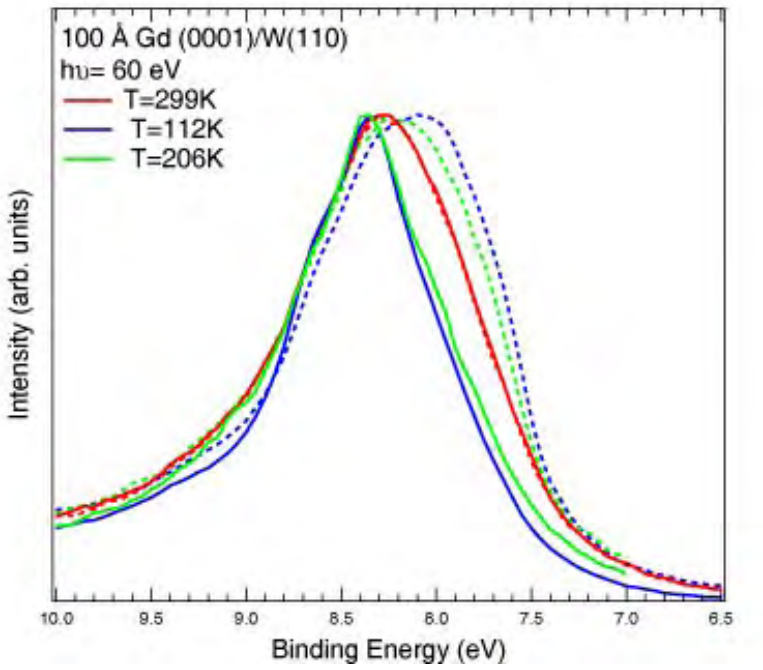

Figure 5.14: Photoemission spectra of the Gd 4f core-level for different temperatures. The solid lines represent photoemission spectra recorded for magnetization up, and the doted lines for magnetization down.

5.4 Ultrafast Magnetization Dynamics

1996 Beaurepaire and coworkers managed to demagnetize a thin Ni film with a strong laser pulse in less than half a picosecond [Bea96]. Similar studies [Bea96, Gui02, Koo03, JYB04] demonstrated that ultrafast demagnetization of thin 3d ferromagnetic films upon optical excitation occurs within a few hundred femtoseconds. The interpretation of the dynamics observed in these experiments in terms of magnetization dynamics remains controversial [Koo03, JYB04]. Nevertheless, there are several indications of a true ultrafast demagnetization. The electron system will equilibrate with the lattice via electron-phonon scattering in the picosecond range. An important channel of the quenching of magnetization in 3d ferromagnets can be a complete transfer of angular momentum to the photon and the lattice.
Several differences between 3d ferromagnets and gadolinium make gadolinium an ideal prototype to study magnetization dynamics. The separation between spins, electrons, and lattice is real, since the magnetic moment of the Gd 4f shell is strongly localized. The 4f couple to the valence electrons by 4f-5d interaction.
This work presents the first experimental investigation of picosecond spin dynamics in the gadolinium 4f core-shell. It aims at an understanding of the temporal evolution of the latter contribution to the magnetization. Concretely, the laser-induced

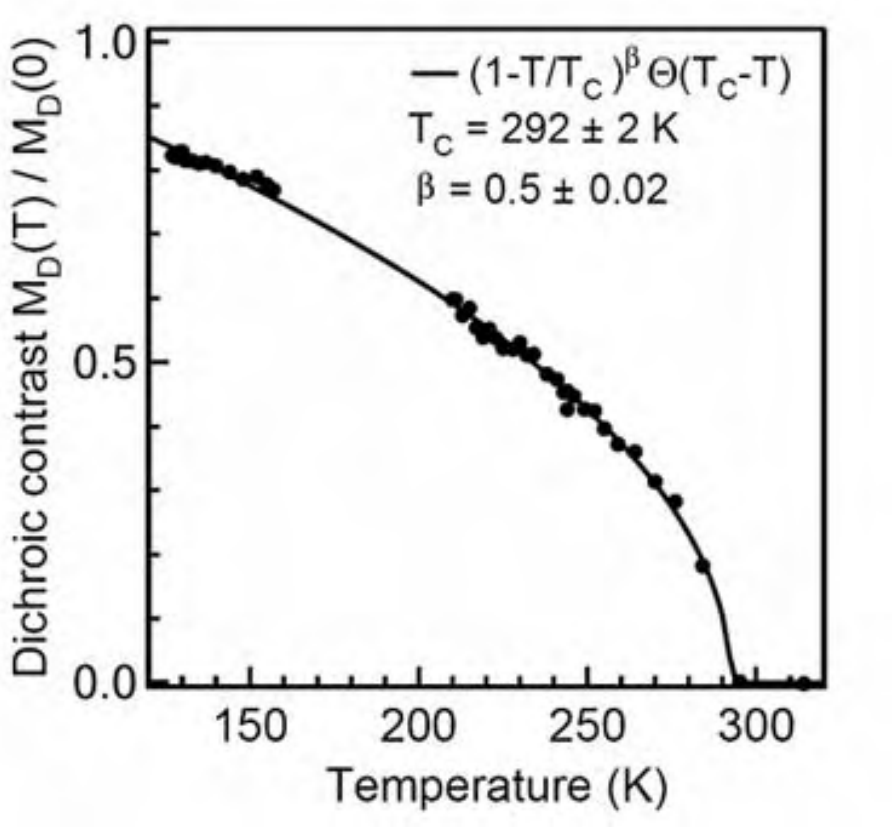

Figure 5.15: Temperature dependence of the MLD for a 100 Å thick Gd films on W(110).

quenching of the magnetic moment of gadolinium directly measured by time-resolved core level spectroscopy of the Gd 4f shell.

5.4.1 Breakdown of the Magnetization at the Gd 4f Shell

Until now all studies of magnetization dynamics in gadolinium have probed the valence-band electrons due to the small photon energies in optical excitation. Non-linear magneto-optical studies demonstrated a breakdown of the magnetization in the surfaces states of gadolinium after laser excitation [Vat91, Vat92, Mel03, Lis05, Bov06]. The main motivation of this research is to investigate the spin dynamics of the 4f core-level electrons.
A combined laser-pump synchrotron-probe experiment permits to reach the 4f core-level and measure directly the transient changes of the linear magnetic dichroism of the Gd 4f photoemission line (Sec. 5.3) reflecting the magnetization dynamics. The experiment has been performed at beamline U125/1 at BESSY using the experimental setup described in Sections 2.3 and 2.4.

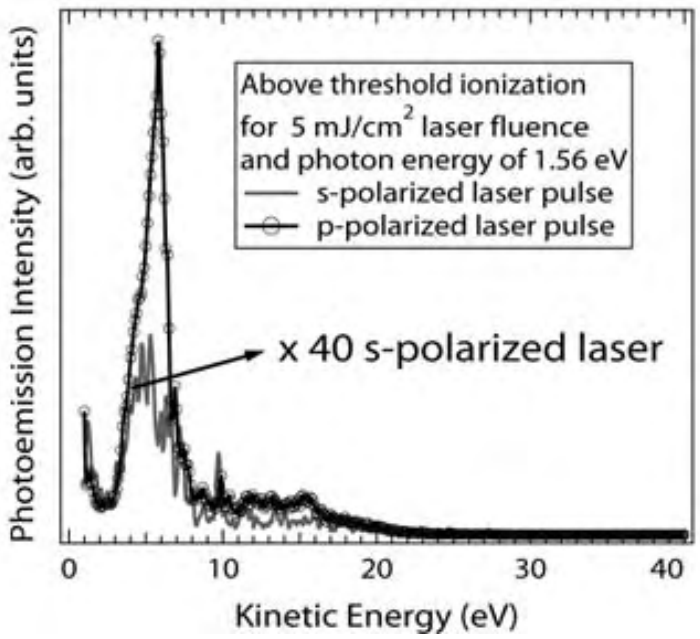

Figure 5.16: Multiphoton processes produced by the laser with p-(dots curve) and s-polarized (solid curve) light with an absorbed excitation fluence of 5 mJ/cm^2.

The pump-laser pulse with a $h\nu = 1.53$ eV photon energy has a duration of 100 fs while the probe-synchrotron-pulse has a duration of about 50 ps in single bunch operation mode (Table 2.1).
Notice that absorption of fs laser pulse with high intensity distorts the photoemission spectra by Coulomb repulsion between the photoemitted electrons. Indications of such a space charge effect (SCE) are the broadening and the shift of the spectrum [Pas06]. Figure 5.16 shows multiphoton ionization processes for p- and s-polarized laser pulses with an absorbed laser fluence of 5 mJ/cm^2. Figure 5.17 depicts 4f core-level spectra recorded at a photon energy of 60 eV and a sample temperature of 80 K. The gadolinium film was remanently magnetized either parallel (dashed line, M $\uparrow$, up magnetization) or antiparallel (solid line, M $\downarrow$, down magnetization) to the z-axis as sketched in Fig. 5.11. Figure 5.17a displays the photoemission spectra (PS) for a long energy range, including the Gd 4f photoemission line, the Fermi level and the surface state. Secondary electrons excited by primary electrons emitted from valence band and surface state contribute to the background of the 4f spectra. Figure 5.17b shows spectra measured without laser excitation, while spectra presented in Fig. 5.17c have been recorded for overlapping laser-pump and synchrotron-probe pulses. The 4f spectral shape and intensity I$\uparrow$ and I$\downarrow$ are different for both magnetization directions M$\uparrow$ and M$\downarrow$, the so-called MLD (Section 5.3).

Three effects arise upon laser excitation, which are visible in Fig. 5.17c, first, the

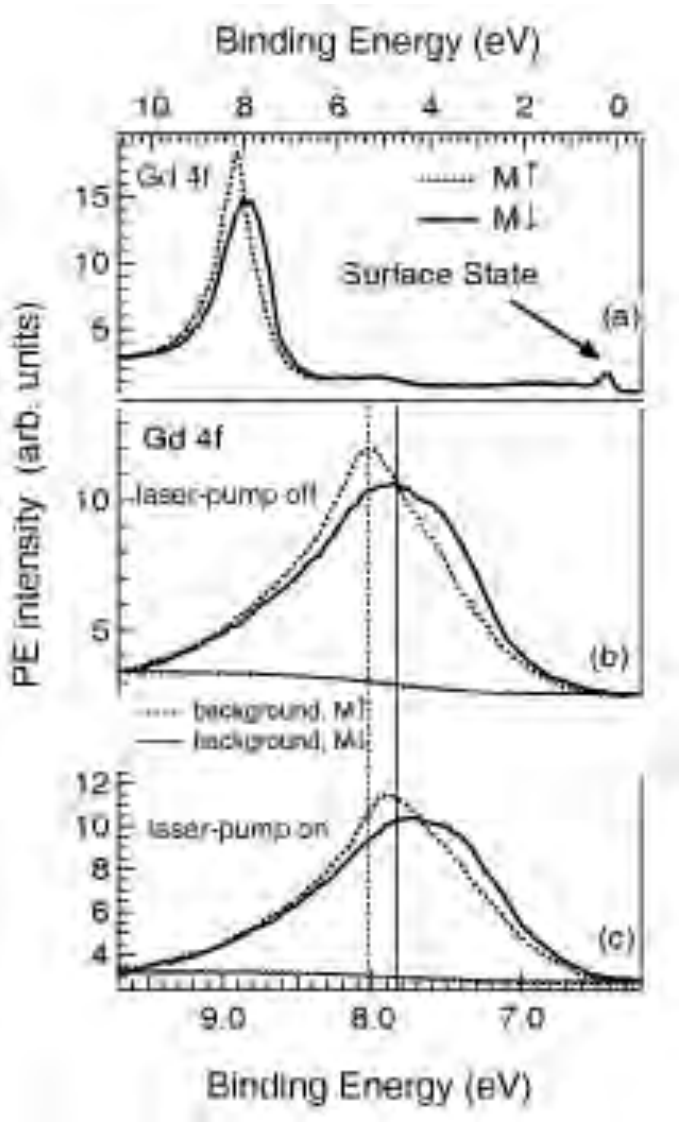

Figure 5.17: Photoemission spectra for magnetization up and down of a 100 Å thick Gd(0001) film on W(110). a) Overview. b) Without laser excitation. c) Overlapping pump and probe pulses.

spectra shift to lower binding energy, second they slightly broaden and third the overall dichroic signal decreases. Subtracting a Shirley background from the raw data in Fig. 5.17 we calculate the average and the dichroic spectra, according to:

$$S_D = \frac{I\uparrow - I\downarrow}{2} \quad \text{dichroic spectrum} \tag{5.17}$$

$$S_A = \frac{I\uparrow + I\downarrow}{2} \quad \text{average spectrum} \tag{5.18}$$

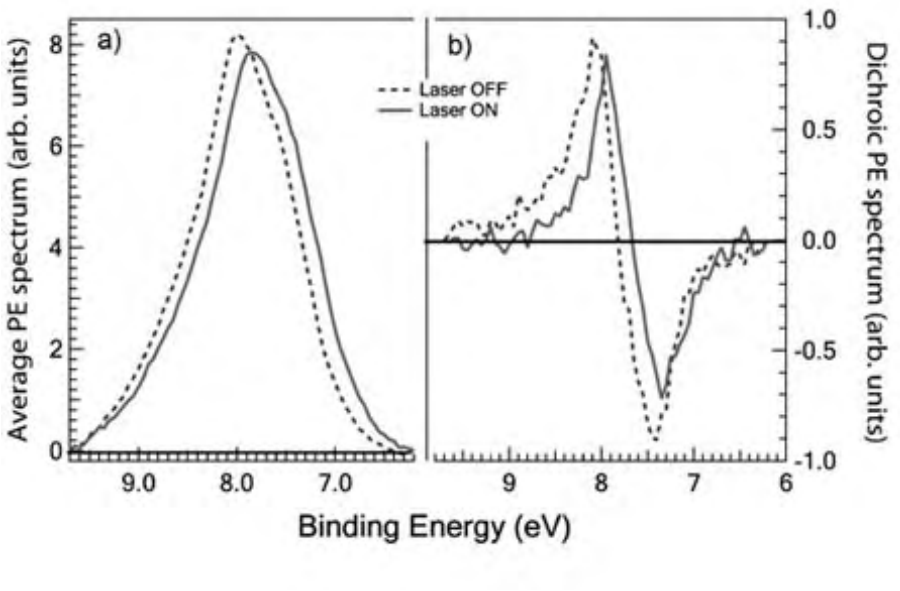

Figure 5.18: Dichroic and average photoemission spectra for a 100 Å thick Gd(0001) film on W(110). a) Average spectra with and without optical excitation the average spectra have been calculated after subtraction of a Shirley background. b) MLD of the Gd 4f core-level with and without optical excitation (solid and dots lines).

The shift to lower binding energies and the broadening of the spectra are attributed to SCE. In order to separate these effects from the decrease of the dichroic signal, the temporal evolution of the peak shift has been analyzed calculating the mean value (center of mass)

$$E_c = \frac{\int E\ S_A(E)\ dE}{\int S_A(E) dE} \tag{5.19}$$

and the width via the mean squared deviation

$$W = \sqrt{\frac{\int (E - E_c)^2\ S_A\ (E) dE}{\int S_A(E) dE}} \tag{5.20}$$

The pump-induced shift and broadening are calculated from these values

$$\Delta E = E_C^{ON} - E_C^{OFF} \tag{5.21}$$

$$\Delta W = \frac{W^{ON} - W^{OFF}}{W^{OFF}} \tag{5.22}$$

Figure 5.19a and b displays the temporal evolution of the pump-induced peak shift and broadening. The peak shift does not affect the evaluation of the magnetic dichroism. While the most critical effect is the broadening will affect. As will be

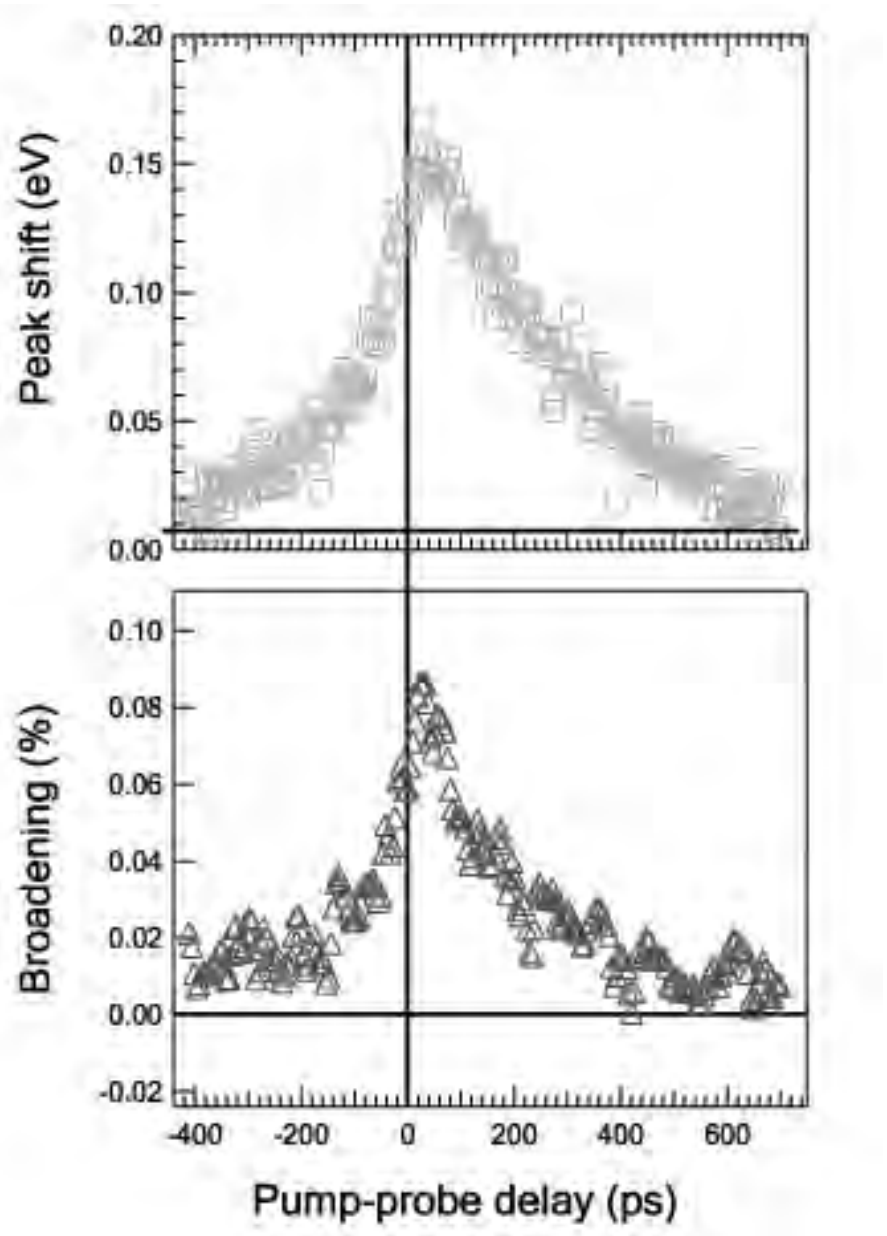

Figure 5.19: a) Temporal evolution of the pump-induced peak-shift of the Gd 4f core-level. b) Temporal evolution of the pump-induced broadening of the spectra.

shown below the temporal evolution of the broadening produced by the pump-laser can be neglected compared to the quenching of the magnetic moment.

The dominant effect is the decrease of the magnetic dichroic signal for overlapping laser and synchrotron pulses as presented in Fig. 5.17 recorded for 3.5 mJ/cm^2

absorbed pump fluence. For each delay between laser and synchrotron the dichroic contrast was calculated as:

$$M_D = \sqrt{\frac{\int dE \cdot S_D^2(E)}{\int dE \cdot S_A^2(E)}} = \sqrt{\frac{\int dE \cdot s_D^2(E)}{\int dE \cdot S_A^2(E)}} \cdot \; M \equiv \gamma \cdot \; M \tag{5.23}$$

where it is assumed $S_D(E) = s_D(E) \cdot \; M$, s_D represents the spectral line shape of the dichroic spectrum and M the total magnetic moment of the 4f shell. As already mentioned the magnetic dichroic signal M_D has been also measured as a function of the temperature. It shows a typical ferromagnetic behavior and in particular decreases to zero at the Curie temperature T. This suggests that the dichroic signal indeed reflects the magnetization of the sample and allows us to monitor the magnetic order of the 4f spin system of gadolinium. The relative pump-induced change

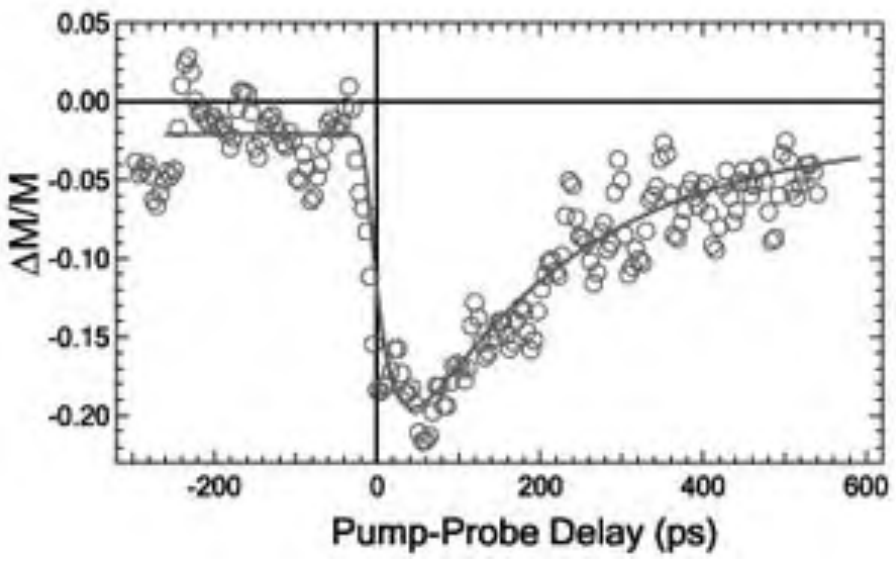

Figure 5.20: For a 100 Å thick Gd(0001) film on W(110). a) Temporal evolution of the pump-induced breakdown of the dichroism versus time delay between laser and synchrotron.

of the magnetic order for delay $\Delta\, t$ between laser and synchrotron pulses is evaluated assuming

$$\frac{\Delta\; M_D(\Delta\; t)}{M_D} = \frac{M_D^{ON}(\Delta\; t) - M_D^{OFF}}{M_D^{OFF}} \tag{5.24}$$

To describe this variation as a function of the pump-probe delay a phenomenological model function is used,

$$f(\tau) = f_0 + (f_1 - f_0)e^{\frac{\tau - \tau_0}{\tau_R}} \tag{5.25}$$

Equation 5.25 was convoluted with a Gauss function, where the FWHM is the temporal resolution of the experiment. From the result of the fit function the recovery

time of the magnetic order is approximately $\tau_R = 255 \pm 30$ ps and the time resolution is $\tau_P = 50 \pm 10$ ps. The relative magnetic contrast is shown in Fig. 5.20. From Eq. 5.24 it follows that the magnetic order only reflects the true magnetization dynamics $\Delta M(\Delta t)/M$ as long as the broadening caused by the SCE is small. While the SCE induced overall shift of the spectra should be independent of the magnetization direction and thus not affect the average dichroic signal, holds only for a homogeneous broadening of the spectrum. Nevertheless, since the relative broadening is significantly smaller than the drop of spin polarization, residual artifacts in $\Delta M(\Delta t)/M$ should be considerably smaller than the SCE itself. Furthermore, while the magnetization shows, a clear drop at zero pump-probe delay (see Fig. 5.20), shift and broadening in Fig. 5.19a and b exhibit a much broader onset. Electrons photoemitted 200 ps before the pump pulse hits the sample are still affected by the space charge created at zero delay, but the magnetization and thus the dichroic contrast remain constant for negative pump-probe delays.

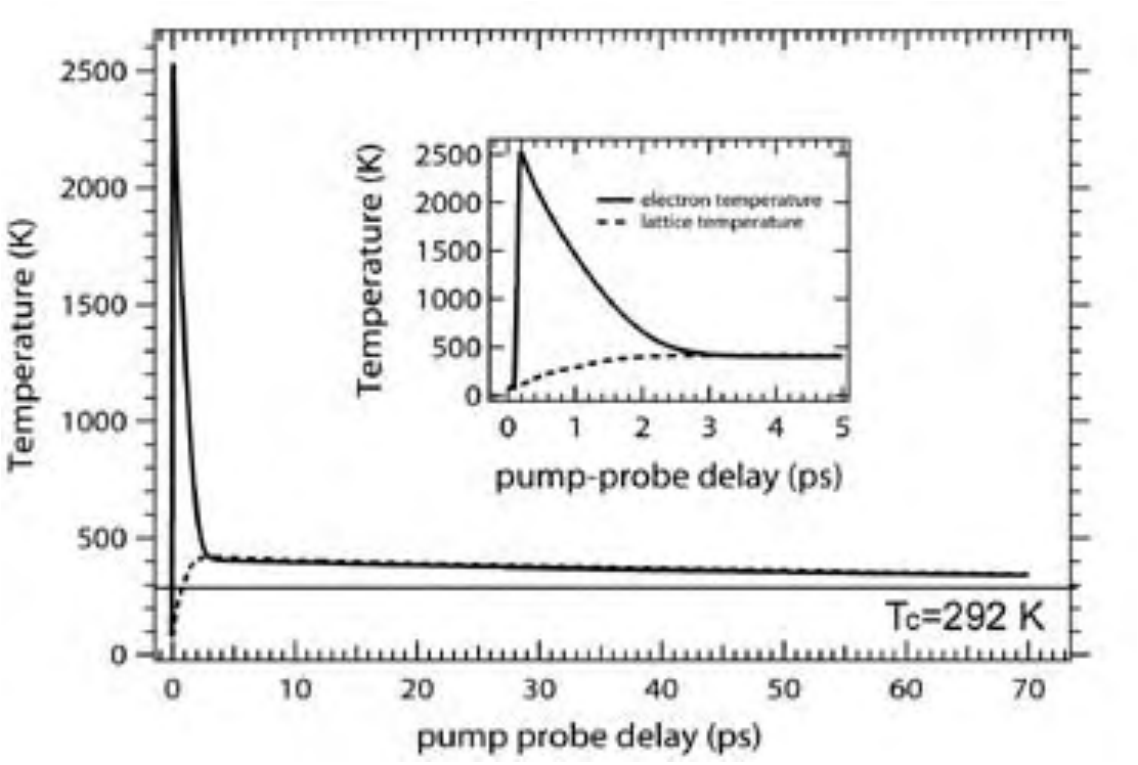

Figure 5.21: Transient evolution of electron and lattice temperature in Gd after optical excitation with laser pulses of 1.5 eV photon energy and for an absorbed pump fluence of 3.5 mJ/cm^2

In conclusion, it has been established that the transient dichroic spectrum of the 4f core-level can be used to monitor the magnetization in gadolinium. The drop

of the magnetization observed upon laser-excitation is about 20%. The magnetization recovers in approximately 250 ps. This timescale is consistent with the early magneto-optical experiments and is attributed to slowly cooling of the lattice after laser-excitation. Unfortunately, the duration of the synchrotron electron-bunches between 40-80 ps in single bunch operation does not allow to unravel the dynamics of ultrafast demagnetization. As the drop in $\Delta M(\Delta t)/M$ simply reflects the time resolution of the experiment it only defines an upper limit of 50 ps in which ultrafast demagnetization occurs. A two-temperature model calculation has been performed for 3.5 mJ/cm^2 absorbed laser fluence even taking into account the influence of the tungsten substrate on the heat diffusion. The result is displayed in Fig. 5.21. The hot electrons excited by the laser beam thermalize with the lattice above the Curie temperature in about 3 ps. Consequently, a single temperature is sufficient to describe the energy content of the two subsystems. The thermalization above the Curie temperature indicates that electrons and phonons are thermalized but not in equilibrium with the 4f spin system. For temperatures above T_C we would expect a complete loss of magnetization $\Delta M = 0$. The ultrafast demagnetization process can not be time resolved. It is expected to be mediated by 4f-5d interaction. Such interactions are based on transient changes of the exchange interaction, the anisotropic character of spin-orbit coupling, and modifications of the magnetic moment due to, e.g., spin-flip processes [Lis04]. Once the 4f spins system is not in equilibrium with the lattice system, the 4f spin can not polarize the valence electrons. This is in agreement with time-resolved magneto-optical studies of the surface state of gadolinium [Lis05], where the magneto-optical response shows a 50% drop of the spin polarization. We conclude that the excited spin system transfers momentum from the valence electrons to the 4f spin system by 5d-4f interaction and the 4f spin system takes more than 50 ps to equilibrate with the lattice.